DOI 10.1007/s11141-023-10208-4
Radiophysics and Quantum Electronics, Vol. 65, No. 4, September, 2022
(Russian Original Vol. 65, No. 4, April, 2022)

RESONANT INTERACTION OF ENERGETIC ELECTRONS WITH RADIO EMISSION IN THE MAGNETOSPHERES OF EXOPLANETS

V. S. Grach* **and A. G. Demekhov** UDC 533.9

We analyze the resonant interaction of energetic electrons with radio emission in the magnetospheres of exoplanets using the planet Tau Bootis b as an example. The conditions of this interaction and its impact on the parameters of electrons are considered for the radio emission which is detectable on the Earth. Specific features of the interaction are studied in comparison with the interaction of energetic electrons with auroral kilometric radiation in the Earth's magnetosphere. It is shown that for the considered parameters of the magnetosphere of Tau Bootis b and radio emission in it, the resonant interaction of electrons with radio emission is strongly nonlinear. For a wave packet of finite duration, the interaction can cause a significant acceleration of particles in a wide range of energies (from tens to hundreds of kiloelectronvolts).

1. INTRODUCTION

One of the topical problems of modern astronomy is the discovery and exploration of planets outside the solar system, namely, exoplanets [1]. The discovery of more than 4500 of exoplanets have been confirmed to date [2], most of which have been detected in the last decade. Interest in various methods of studying the properties of exoplanets and their envelopes is steadily growing.

Planets with a strong magnetic field and a fairly dense atmosphere make up a special group. First of all, these are the so-called hot Jupiters, or planets with masses of the order of 1–10 Jupiter masses and located at a distance of the order of 0.05 a. u. from their star [3–10]. It is known from the results of studying the planets of the solar system that several types of radiation generated by plasma instabilities can be characteristic of the magnetospheres of such planets [11–18]. Such signals can have large amplitudes due to the stimulated nature of the radiation. Therefore, on the one hand, some of them are suitable candidates for detection by ground- and satellite-based tools [5, 10], and on the other hand, these emissions can strongly affect the energetic component of the circumplanetary plasma. Energetic charged particles, in turn, can cause both the heating of the planetary atmosphere (due to precipitation) [19] and intense auroral radiation, which affects the total radiation balance in the ionosphere.

In the magnetospheres of planets, radiation is generated due mainly to resonance effects, in particular, cyclotron–resonance ones; the effect of this radiation on charged particles is of the same nature [13, 15, 17, 20–22]. The Earth's magnetosphere research shows that the cyclotron interaction mechanism is effective both for waves not leaving the magnetosphere (whistler-mode [23–27] and ion–cyclotron waves [28–33]) and for waves forming the radio emission [13, 14, 34–38], among which a fast extraordinary wave (X mode) stands out. Such a resonant interaction appears to be most efficient in the case of quasi-monochromatic signals, for which it becomes strongly nonlinear for a fairly large wave amplitude [31, 32, 39-43].

* vsgrach@ipfran.ru

[1] Institute of Applied Physics of the Russian Academy of Sciences, Nizhny Novgorod, Russia. Translated from Izvestiya Vysshikh Uchebnykh Zavedenii, Radiofizika, Vol. 65, No. 4, pp. 249–268, April 2022. Russian DOI: 10.52452/00213462_2022_65_04_249 Original article submitted October 14, 2021; accepted December 12, 2021.

The magnetospheres of exoplanets may be very different from the Earth's and Jupiter's magnetospheres by their properties. Radio emission from exoplanets that can be detected on the Earth corresponds to high magnetic fields in the exoplanet magnetospheres and high wave amplitudes. Simulation of resonant interaction with radio emission in the exoplanet environment will permit one to follow how nonlinear interaction processes are modified under such conditions.

This work is devoted to the study of the resonant interaction of electrons with radio emission (X mode) in a plasma with parameters corresponding to modern ideas about the magnetosphere of the planet Tau Bootis b (tau boo b, Tau Bootes b), for which conceivable signatures of radio emission were found for the first time [10]. The main purpose of this study is to identify new features of such interaction, which are due to the characteristic parameters of plasma and radiation, and clarify the possibility of efficient energy exchange between charged particles and radiation. It is shown that under the considered conditions the resonant interaction is essentially nonlinear. For a finite duration of the wave packet, it can lead to a significant acceleration of particles with lower energies and a decrease in the energy of particles with higher energies.

This paper is organized as follows. Section 2 gives estimates of the parameters of the magnetosphere and radio emission. Section 3 describes the wave-packet model and analyzes the possibility of resonant interaction in the obtained ranges of parameters. The system of equations describing the interaction of radio emission with energetic electrons is given in Sec. 4. The results of calculating the interaction of the model packet with energetic electrons are given in Sec. 5. Section 6 formulates the main results of the work.

2. ESTIMATES OF THE POSSIBLE PARAMETERS OF THE PLANET'S MAGNETOSPHERE AND RADIO EMISSION

The parameters of the planetary magnetic field and the properties of the atmosphere have been estimated for many hot Jupiters [3–9]. Herein, the radio emission generated during cyclotron radiation of charged particles can escape from the planet's magnetosphere, according to estimates [9], for the supermassive hot Jupiter Tau Bootis b. Signatures of radio emission from this planet have also been found on the Earth [10]. Therefore, in this paper, the possible resonant interaction of radio emission with energetic electrons is analyzed for Tau Bootis b.

2.1. Parameters of the planet's magnetosphere

According to estimates [4], the planet has a radius $R_\mathrm{p} = 1.06R_\mathrm{J}$ and a magnetic moment $M = 0.76M_\mathrm{J}$, where R_J and M_J are the radius and magnetic moment of Jupiter, respectively. Based on other papers, the magnetic moment of the planet can amount to $2.8M_\mathrm{J}$ [5] or $7.5M_\mathrm{J}$ [6].

According to [9], the magnetospheric plasma density at a distance of 0.10–$0.15R_\mathrm{p}$ from the planet surface (in the exobase region) is 10^6 cm^{-3}. No data are given on the plasma-density profile above the exobase, but it is assumed that this profile is similar to that in the Jovian magnetosphere, i. e., the plasma density continues to decrease fairly rapidly to less than 10^4 cm^{-3}. Thus, the dense plasma region in the magnetosphere is relatively small in size.

2.2. The parameters of radio emission

Based on estimates [10], radio emission is observed in the range 14–30 MHz, and the radiation flux is higher in the range 14–21 MHz.

Wave amplitude in the planet's magnetosphere can be estimated as follows. The minimum radiation flux measured with most ground-based telescopes is 10 mJ, i. e., the radiation flux from Tau Bootis b can be written as

$$J_{\tau\mathrm{b}} = \alpha \cdot 10 \text{ mJy} = \alpha \cdot 10^{-25} \text{ cgs}. \quad (1)$$

According to the results in [10], the coefficient α is equal to 1–100.

The relation between the amplitude of the wave electric field E at the output of the generation region and the radiation flux at the telescope has the form

$$\frac{E^2[\mathrm{cgs}]}{8\pi} = \frac{J_{\tau\mathrm{b}}[\mathrm{cgs}]f[\mathrm{Hz}]}{c[\mathrm{cm/s}]}\left(\frac{L_{\mathrm{source}}}{R_{\mathrm{source}}}\right)^2. \tag{2}$$

Here, L_{source} is the distance to the source, R_{source} is the conditional source size, f is the radiation frequency, and c is the speed of light in empty space. For the planet Tau Bootis b, $L_{\mathrm{source}} = 15.6$ pc (distance to the corresponding star), R_{source} can be estimated as $R_{\mathrm{source}} = \beta R_{\mathrm{p}} = 1.06\ \beta R_{\mathrm{J}}$ and the frequency f, as $f = \delta \cdot 10$ MHz. Here, the coefficients β and δ are of the order of unity.

For the values mentioned above, we have

$$E[\mathrm{V/m}] \approx 5\frac{\sqrt{\alpha\delta}}{\beta}. \tag{3}$$

As was mentioned in the Introduction, nonlinear interaction with discrete signals, i. e., quasi-monochromatic wave packets of finite duration, can be most efficient. Observation of the fine structure of the auroral kilometric radio emission (AKR) in the Earth's magnetosphere were analyzed in [44–47]. According to [47], the duration of AKR packets with frequencies of up to 400 kHz ranges from 0.2 to 4 s. To estimate the possible duration of radio emission pulses in the magnetospheres of other planets, we will use the conclusions of the discrete-signal generation theory developed in the most detailed way for chorus emissions in the Earth's magnetosphere. According to theoretical estimates confirmed by the satellite data analysis [48–50], the minimum packet duration τ_{min} is equal to the inverse of the electron oscillation frequency in the wave field near the minimum of the effective potential of the wave (trapping frequency $f_{\mathrm{tr}} = \Omega_{\mathrm{tr}}/(2\pi)$),

$$\Omega_{\mathrm{tr}}^2 = |1 - 1/(n^2\cos^2\chi)|\frac{e\omega n^2\cos^2\chi V_\perp |E|}{mc^2\gamma}. \tag{4}$$

Here, $\omega = 2\pi f$, χ, and n are the angular frequency, the wave-normal angle, and the refractive index of the wave, respectively, $e > 0$ is the elementary charge, and m, γ, and $V_\perp$ are the electron rest mass, Lorentz factor, and velocity transverse to the external magnetic field, respectively.

Assume that the ratio between the wave packet duration and the frequency f_{tr} ($\tau_{\mathrm{min}} \sim f_{\mathrm{tr}}^{-1}$) is also fulfilled for AKR. Since the dependence of f_{tr} on the frequency amd amplitude of the wave field for the Z mode is the same as for whistler-mode waves (4), it can be assumed that in this case $\tau_{\mathrm{min}}^{-1} \propto \sqrt{fE}$ (we suppose that for AKR $n^2 \sim 1$). Then, if, according to [47], we believe that a wave packet with a frequency of about 300 kHz has a duration of 0.2–2.0 s and estimate the AKR amplitude as 0.5 V/m, then the minimum duration of such a packet in the magnetosphere of Tau Bootis b will amount to

$$\tau_{\mathrm{min}}[\mathrm{s}] = \frac{(0.008\text{–}0.08)\beta^{1/2}}{\alpha^{1/4}\delta^{3/4}}, \tag{5}$$

where the coefficients α, β, and δ are the same as in Eq. (3).

3. CHOOSING PARAMETER VALUES FROM THE POINT OF VIEW OF THE RESONANT INTERACTION EFFICIENCY

3.1. Features of the resonant interaction

Under the conditions of the Earth's magnetosphere, the AKR generation region is located at high geomagnetic latitudes and altitudes of 5000–15000 km. In this region, the geomagnetic field can approximately be considered as dipole. By analogy with papers [37, 38], we also assume that the magnetic field of the planet Tau Bootis b is dipole in the region of resonant interaction of electrons with radio emission.

For convenience, in the further analysis the position of particles and waves in space will be denoted by the distance h from the surface of the planet along its magnetic field $\mathbf{B}_0$; in the region under consideration, the field B_0 decreases monotonically as h increases.

Following the existing ideas about the generation of radio emission in the magnetospheres of the Earth and Jupiter, we assume that radio emission with a frequency ω is a fast extraordinary wave (X mode) and is generated in the vicinity of the point where the angular frequency $\omega = 2\pi f$ of the wave coincides with the local cutoff frequency $\Omega_{\rm X}$. Correspondingly, the X mode can only propagate in the region $\omega > \Omega_{\rm X}$, i. e., from the planet. In a cold plasma,

$$\Omega_{\rm X} = \frac{\Omega_{\rm c}}{2}\left(1 + \sqrt{1 + \frac{\Omega_{\rm p}^2}{\Omega_{\rm c}^2}}\right) > \Omega_{\rm c}. \tag{6}$$

Here, $\Omega_{\rm p}$ and $\Omega_{\rm c}$ are the plasma frequency and gyrofrequency of electrons, respectively. The difference between $\Omega_{\rm X}$ and $\Omega_{\rm c}$ is small, i. e., it can be assumed that the highest possible frequency of the considered wave is determined by the gyrofrequency of electrons near the surface of the planet.

In our previous works [37, 38], the wave-normal angle χ was considered constant during the wave propagation. In this paper, we consider a more realistic model taking refraction into account. We neglect the transverse inhomogeneity of the medium and displacement of the beam across the magnetic field. In this case, where the inhomogeneity of the medium is smooth and one-dimensional, Snell's law is fulfilled during the wave propagation: $n(\chi)\sin\chi = \text{const} = \sin\chi_{\rm c}$, where $\chi_{\rm c}$ is the wave-normal angle in the region $n \to 1$. Such a wave can exist in the region $h > h_{90} > h_{\rm X}$, where $n(h_{90}) = \sin\chi_{\rm c}$, and the quantity $h_{\rm X}$ characterizes the point where the condition $\omega = \Omega_{\rm X}$ is fulfilled (hereafter, the cutoff point).

Since the refractive index for the X mode monotonically increases with increasing distance from the cutoff point, then the smaller $\chi_{\rm c}$, the closer to the cutoff point the wave generation can start. In this case, as the wave propagates towards the larger values of n, the wave-normal angle χ decreases, while $\chi = 90^\circ$ at the point h_{90}. Allowance for refraction does not qualitatively affect the resonant-interaction properties considered in [37, 38].

The relativistic condition for the fundamental cyclotron resonance is written as

$$\Delta = \omega - \omega n \cos\chi V_{||}/c - \Omega_{\rm c}/\gamma = 0, \tag{7}$$

where $V_{\|}$ is the electron velocity component along the external magnetic field. Since for the X mode $\omega > \Omega_{\rm X} > \Omega_{\rm c}$, condition (7) can only be fulfilled for co-moving electrons in a limited energy range and in a certain vicinity of the cutoff point.

A distinctive feature of the resonant interaction with the X mode is a nonmonotonic dependence of the detuning Δ on the magnitude of the external magnetic field when the particle moves in the direction of its decrease [37]. As a consequence, there are two resonance points. In what follows, the first point will be called the point which is located closer to the cutoff point (and, accordingly, the surface of the planet). Depending on the parameters of the wave and the electron, the vicinities of these two points can represent both one common resonant interaction area and two independent ones.

3.2. Analysis of the possibility of resonant interaction

We now analyze the possibility of resonant interaction for various values of the magnetic moment of the planet and the plasma density in the magnetosphere (Sec. 2.1). For definiteness, we confine ourselves to the geomagnetic latitude 70°.

For the lowest magnetic moment $M_1 = 0.76M_{\rm J}$, the wave frequency $f < 10$ MHz, i. e., in this case, the radio emission cannot be detected on the Earth's surface; so, in what follows we analyze only the magnetic moments $M_2 = 2.8M_{\rm J}$ [5] and $M_3 = 7.5M_{\rm J}$ [6]. We also consider three electron-density models, in which $N_{\rm e} = 10^6$ cm^{-3} per $0.1R_{\rm p}$ [9] and then decreases proportionally to the magnetic field and $N_{\rm e} = 10^5$ cm^{-3} or 10^4 cm^{-3} per $0.2R_{\rm p}$ and then decreases proportionally to the magnetic field.

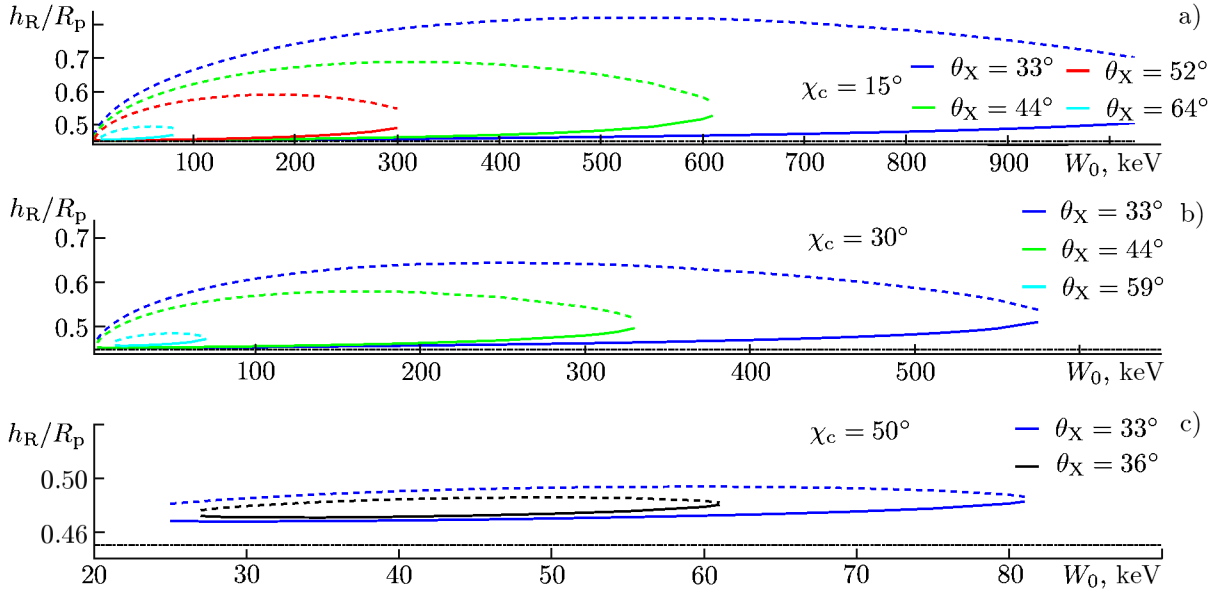

Fig. 1. Position of the resonance points as a function of the electron energy W_0 and pitch angle θ_X for different values of the angle χ_c. The angle $\theta_X = 33°$ corresponds to the opening angle of the loss cone. The black line shows the position of the cutoff point h_X.

Test calculations show the following. Resonant interaction of electrons with X-mode wave is possible if the wave frequency exceeds a certain minimum frequency f_{min}, and the wave-normal angle in the interaction region is less than some maximum angle χ_{max}. Herein, f_{min} increases with increasing magnetic moment M and electron density N_e, while χ_{max} increases with increasing M and decreases with increasing N_e. In the case of the highest density $N_e = 10^6$ cm^{-3}, the resonant interaction is possible only for $M = M_3$.

For the further analysis, we choose the case where $M = M_2$ and $N_e = 10^5$ cm^{-3}. Relying on the data in [10], we choose the wave frequency $f = 20$ MHz.

3.3. Resonant values of the electron parameters

Let us analyze the range of resonant values of the electron parameters (energy and pitch angle) for the specified parameters of the magnetosphere at $f = 20$ MHz and various values of the limiting wave-normal angle χ_c (corresponding to the region $n \approx 1$). With allowance for refraction, the interaction is possible for wave-normal angles $\chi_c \leq 50°$.

Figure 1 shows the dependences of the positions of both resonance points h_R on the electron energy W_0 and the pitch angle at the cutoff point θ_X for three angles χ_c.

Qualitatively, the dependences $h_R(W_0, \theta_X), \chi_c))$ look similar to the case of AKR in the Earth's magnetosphere [37]. For a fixed θ_X, the resonance points merge at the boundaries of the resonant-energy range; the largest distance between them corresponds to the middle of this range. The distance to the first resonance point has a minimum and the distance to the second point, a maximum, depending on the energy (for a fixed θ_X). Herein, the resonance point for the maximum resonant energy is located farther from the cutoff point than the resonance point for the minimum resonant energy.

As θ_X increases, the distance between resonance points decreases and the resonant-energy range becomes narrower (the minimum resonant energy slightly increases and the maximum resonant energy decreases significantly). As the wave-normal angle χ_c increases, the range of resonant values of the electron parameters also reduces, that is, the maximum resonant pitch angle decreases, the minimum resonant energy slightly increases, and the maximum resonant energy reduces significantly. In addition, as χ_c increases, the distance between resonance points decreases and the distance from the cutoff point to the first resonance point increases.

It should be noted that the maximum distance between resonance points for the considered parameters is about $3 \cdot 10^4$ km $\approx 2 \cdot 10^6 c/f$. For the AKP parameters considered in [37, 38], the maximum distance between resonance points was approximately $3 \cdot 10^3$ km $\approx 6 \cdot 10^4 c/f$. Thus, under the conditions of the Tau Bootis b magnetosphere, the distance between the resonance areas in units of wavelength is much larger than in the Earth's magnetosphere.

3.4. Interaction with wave packets of finite duration

As in [37, 38], we consider interaction with a wave packet of finite duration. The propagation of a packet is calculated in the geometrical-optics approximation. Let at the initial time $t = 0$ the trailing edge of the packet has some coordinate $h_{\rm gen}$ along the planetary magnetic field line, and the leading edge is located at a distance $L_{\rm p}$ from it (along the planetary magnetic field line).

When calculating the propagation of a wave packet, the group velocity of each element along the planetary magnetic field is determined by solving the dispersion relation for cold plasma corresponding to a fast extraordinary wave, while the components of the electric and magnetic fields are interconnected by the corresponding polarization relations. We believe that in the region $n \approx 1$ the condition $\chi = \chi_{\rm c} = {\rm const}$ is fulfilled. It follows that $n \sin\chi = {\rm const} = \sin\chi_{\rm c}$ for all points of the packet at any instant of time.

According to the widespread ideas about the AKR generation [34, 51], the wave-normal angles are fairly high in the generation region. We assume that the point $h_{\rm gen}$ corresponds to the wave-normal angle $\chi_{\rm gen} = 89^\circ$. A decrease in $\chi_{\rm gen}$ will reduce the range of electron parameters for which efficient interaction is possible, but for $\chi_{\rm gen} \geq 80^\circ$ this effect is not significant.

One of the reasons why the finite length and evolution of the wave packet edges are important factors in the interaction with energetic electrons is that the group velocity of the X mode is comparable with the velocity of resonant electrons in the interaction region. This means that the electrons should be in the interaction region in a small time interval relative to the wave packet generation time. Namely, if the electron flies through the resonance region too early, there will be no packet in it yet and if it is too late, the wave packet will already have moved beyond the resonance region. Also, a case is possible where the electron is in the packet only in the vicinity of the first resonance point (the packet is too short or the electron has an "early start") or only the second one (the electron has a "late start").

In the model considered, the wave packet with a lower wave-normal angle $\chi_{\rm c}$ leaves the resonant-interaction region faster and will have a shorter duration for a fixed length $L_{\rm p}$ at the initial instant of time. This is due to the fact that the initial position of the trailing edge of the packet (generation point) for a fixed $\chi_{\rm gen}$ is determined by the value of $\chi_{\rm c}$. For higher angles $\chi_{\rm c}$, the generation point is located farther from the cutoff point, i. e., in the region of a higher refractive index and a higher group velocity. The situation is reverse in the refractionless model considered in [37, 38] under the condition that the wave packets are generated at one point: the packets with a higher angle χ have a longer duration and are slower to leave the resonant-interaction region.

For the $\chi_{\rm c}$ values considered in Sec. 3.3, we have the following estimates of the wave packet duration from the point of view of the efficiency of resonant interaction. For the wave-normal angle $\chi_{\rm c} = 15^\circ$, the interaction in both zones of resonance is possible for electrons with energies in most of the range indicated in Fig. 1 if the packet duration exceeds $\tau_{\rm full} = 0.45$ s. The minimum wave packet duration with which interaction is possible in the vicinity of at least one resonance point for a wide range of resonant energies is $\tau_{\rm min} = 0.25$ s. In this case, the packet leaves the first resonance zone over the time $\Delta t^{(1)} = 0.45$ s and the second zone, over the time $\Delta t^{(2)} = 0.65$ s. The time scales are $\tau_{\rm full} = 0.3$ s, $\tau_{\rm min} = 0.15$ s, $\Delta t^{(1)} = 0.3$ s, and $\Delta t^{(2)} = 0.42$ s for $\chi_{\rm c} = 30^\circ$ and $\tau_{\rm full} = 0.11$ s, $\tau_{\rm min} = 0.08$ s, $\Delta t^{(1)} = 0.11$ s, and $\Delta t^{(2)} = 0.14$ s for $\chi_{\rm c} = 50^\circ$.

Note that for the Earth's magnetosphere, wave packets with a duration of 0.2 to 2.0 s [47] are "long" from the point of view of efficient resonant interaction, i. e., they cover the entire zone of resonant interaction for the entire range of resonant energies and pitch angles of electrons [37] (as was noted in the previous section, the distance between resonance points in units of wavelengths under conditions of the magnetosphere of Tau

Bootis b is much greater than in the Earth's magnetosphere).

Another important difference between wave packets of finite duration and a monochromatic wave is the possibility of a frequency drift and complex amplitude profile in such wave packets. When studying the Earth's magnetosphere, it was shown that frequency drift plays a significant role in the interaction of electrons with discrete signals of chorus emission [42, 52] or wave packets of electromagnetic ion–cyclotron waves [43, 53]. The results of observations of the fine structure in the AKR [47] also show the presence of a frequency drift in wave packets, but, according to quantitative estimates [37], this drift does not significantly affect the characteristics of the resonant interaction. Therefore, as in [37, 38], we restrict ourselves to wave packets with a constant frequency. Wave-packets with a constant amplitude were analyzed in [37, 38]. Here, we consider a more realistic Gaussian amplitude profile.

4. PROBLEM FORMULATION

4.1. Resonant interaction model

Basic equations and some reference information on interaction regimes were discussed in detail in our previous papers [37, 43] and are given here for the reader's convenience.

The system of equations describing the motion of an electron in a given electromagnetic wave field $\boldsymbol{\mathcal{E}}_{\rm w}$, $\boldsymbol{\mathcal{B}}_{\rm w}$ in the presence of an external magnetic field $\mathbf{B}_0$, consists of the law of conservation of electron energy W, equations for the first adiabatic invariant $I_\perp = p_\perp^2/(mB_0)$ and gyration phase φ, and the law of motion of the Larmor center [37, system (1)–(4)]. For analysis of resonant effects in the electron–wave interaction, this system can be transformed by using the expansion of the electromagnetic field near the center of the Larmor circle [54, 55]. As in [37, 38], we consider interaction only at the fundamental cyclotron resonance. In this case, the position of the particle in the phase space is determined by $z, W, I_\perp$, and Ψ, where z is the coordinate along the field $\mathbf{B}_0$, $\Psi = -\int \omega {\rm d}t + \varphi + \int k_{||}\,{\rm d}z + \phi$ is the phase of the particle relative to the wave (ω and $k_{||}$ are the frequency and longitudinal wave number of the wave, respectively, and ϕ is the constant):

$$\frac{{\rm d}W}{{\rm d}t} = e\frac{p_\perp}{m\gamma}\left[\frac{E_x - E_y}{2}J_0(\kappa) + \frac{E_x + E_y}{2}J_2(\kappa)\right]\sin\Psi + e\frac{p_{||}}{m\gamma}E_z J_1(\kappa)\sin\Psi, \tag{8}$$

$$\frac{{\rm d}I_\perp}{{\rm d}t} = -\frac{ep_\perp}{mB_0}\left[\left(\frac{E_x - E_y}{2} + \frac{p_{||}}{m\gamma c}\,\frac{B_x - B_y}{2}\right)J_0(\kappa) + \left(\frac{E_x + E_y}{2} - \frac{p_{||}}{m\gamma c}\,\frac{B_x + B_y}{2}\right)J_2(\kappa)\right]\sin\Psi, \tag{9}$$

$$\frac{{\rm d}\Psi}{{\rm d}t} = -\Delta + e\left[\left(\frac{E_x - E_y}{2} + \frac{p_{||}}{m\gamma c}\frac{B_x - B_y}{2}\right)J_0(\kappa) - \left(\frac{E_x + E_y}{2} - \frac{p_{||}}{m\gamma c}\frac{B_x + B_y}{2}\right)J_2(\kappa) + \frac{p_\perp}{m\gamma c}B_z J_1(\kappa)\right]\frac{\cos\Psi}{p_\perp}, \tag{10}$$

$$\frac{{\rm d}z}{{\rm d}t} = \frac{p_{||}}{m\gamma}. \tag{11}$$

Here, m and $\mathbf{p}$ are the electron rest mass and momentum, respectively, the indices $||$ and $\perp$ denote projections onto the direction along and across the geomagnetic field $\mathbf{B}_0$, respectively, $\gamma = \sqrt{1 + [p/(mc)]^2} = W/(mc^2) + 1$, $\Omega_{\rm c} = eB_0/(mc)$ is the nonrelativistic gyrofrequency, E_j, B_j $(j = x, y, z)$ are components of the slowly varying complex amplitude of the electromagnetic wave field, which are connected by local polarization relations, the x axis is directed along $\mathbf{k}_\perp$, $\mathbf{k}$ is the wave vector, $J_q(\kappa)$ is a Bessel function of order q, $\kappa = \omega n \sin\chi p_\perp/\Omega_{\rm c}$, $n = kc/\omega$ is the refractive index, χ is the wave-normal angle, $\Delta = \omega - \omega n\cos\chi V_{||}/c - \Omega_{\rm c}/\gamma$ is the detuning from resonance, and $V = p/\gamma$ is the electron velocity. Note

that in system (8)–(11) the quantities B_0 and Ω_c and the characteristics of the wave depend on the spatial coordinate z, and the components of the wave field also depend on the time t. When deriving system (8)–(11), the following assumptions are used: the inhomogeneity of the external field is smooth, the wave amplitude is small ($\mathcal{B}_w \ll B_0$), and wave characteristics in time and space change slowly compared to scales $2\pi/\Omega_c$ and $2\pi/k$, respectively.

The regime of the resonant interaction is determined by the effective inhomogeneity parameter $\mathcal{R} = \sigma_R R$, where $\sigma_R = \pm 1$ determines the sign of the effective inhomogeneity, while

$$R = \frac{|\mathrm{d}\Delta/\mathrm{d}t|}{\Omega_{tr}^2}. \tag{12}$$

Here, $\mathrm{d}/\mathrm{d}t = \partial/\partial t + V_{||}\partial/\partial z$, where differentiation is performed only for the functions z and t, excluding W and $I_\perp$, Ω_{tr}^2 is the squared electron oscillation frequency in the wave field near the minimum of the effective potential of the electron in the wave field (4). Under real conditions, the parameter R varies both in time and space. Moreover, these variations are due not only to the inhomogeneity of the medium and the variation in frequency and amplitude of the wave packet, but also to a nonlinear variation in the parameters of the particles under the action of the wave. However, the main features of the motion can be classified proceeding from the magnitude of R calculated in the resonance region in the linear approximation. Herein, the characteristics of possible interaction regimes are determined both by the value of R and the sign of σ_R.

In the case $R < 1$, the effective potential of a particle in the wave field has a minimum [39]. Herein, trapping of particles by the wave is possible.

In the case $R \gg 1$, the motion of a particle can be considered linear. Integral variation in energy and adiabatic invariant of an electron over the of the resonance region is determined by the phase at the resonance point, which, in turn, depends linearly on the initial phase. For an ensemble of particles, uniformly distributed over the initial phase, the average variation in W and $I_\perp$ is zero, but there is diffusion in the phase space [37, 40, 41, 56].

For $R < 1$, a nonlinear regime takes place, which is characterized by the phase bunching of electrons and non-zero average variation in W and $I_\perp$, both for particles trapped by the wave field and for untrapped particles. In the case $R \ll 1$, a bunching regime occurs for untrapped electrons, in which the variation in energy (and/or adiabatic invariant) is small, almost does not depend on the initial phase of the particle, and has a sign opposite to the sign of energy variation in the trapping regime [40, 41, 43]. Variation of the electron parameters in the trapping regime can be quite significant [40–43].

For interaction with the X mode at the fundamental cyclotron resonance, we have [37]

$$\mathcal{R}^{(1)} > 0, \mathcal{R}^{(2)} < 0. \tag{13}$$

At the boundaries of the resonant-energy range (with a fixed pitch angle) $R^{(1)} \approx R^{(2)} \to 0$. For a constant wave amplitude, the absolute values of $R^{(1)}$ and $R^{(2)}$ have a maximum approximately in the middle of the range of resonant energies and $R^{(1)} < R^{(2)}$.

In the bunching regime, particles lose energy in the first resonance zone and are accelerated in the second one. In the trapping regime, accordingly, the energy picks up in the first zone and decreases in the second one. Herein, at a constant amplitude, as was shown in [37], particle trapping always occurs in the first resonance region and the exit from trapping takes place after passing the second region. For close values of $R^{(1)}$ and $R^{(2)}$, the resulting energy variation is small.

For the indicated parameters of the magnetosphere of Tau Bootis b and the wave with a frequency of 20 MHz and a limiting wave-normal angle $\chi_c = 30°$, the condition $R^{(1)}, R^{(2)} < 1$ will be satisfied for the entire range of resonant values of W_0 and Θ_X for the electric-field amplitude $E \geq 0.5$ V/m at the resonance points.

The considered interaction partially or completely occurs in the radio emission generation region. If we assume that the radio emission in the magnetosphere of Tau Bootis b is generated as a result of cyclotron

instability (this is an AKR generation mechanism, as is commonly accepted), then the non-self-consistent consideration of resonant interaction, which does not take into account the effect of electrons on the wave profile, is only a zero approximation. However, such an approach reveals the expected maximum effects of resonant interaction of energetic electrons with radio emission.

4.2. Simulation parameters

Based on the estimates in Secs. 1 and 2, for a detailed analysis of interaction regimes we have chosen a wave packet with the limiting wave-normal angle $\chi_c = 30^\circ$, a duration of 0.15 s and a Gaussian amplitude profile with the maximum value 5 V/m. In this case, efficient resonant interaction is possible in a wide range of electron energies, and the indicated values of duration and amplitude seem realistic (see Eqs. (3) and (5)). With this amplitude profile, except for cases where the resonance points are located in a small vicinity of one of the packet edges, the conditions $R^{(1)} \ll 1$ and $R^{(2)} \ll 1$ will also be satisfied.

System (8)–(11) was solved numerically for one value of the pitch angle $\Theta_X = 44^\circ$ (which roughly corresponds to the middle of the Θ_X resonant range) and 8 energy values. It was assumed that the ensemble of electrons is located at the point h_{gen} corresponding to the initial position of the trailing edge of the wave packet, at the time $t_0 \geq 0$, i. e., the electrons start moving at the same time with the packet or later (recall that the considered resonant interaction is possible only for co-moving electrons). For each energy value, we have also chosen from 5 to 7 values of t_0 in the interval $0 \leq t_0 < \Delta t_2 = 0.42$ s. For fixed values of W_0, Θ_X, and t_0, 900 values of the initial phase Ψ_0 uniformly distributed in the interval $[0, 2\pi)$ were specified.

The chosen values of W_0, Θ_X, and t_0 permit one to show all possible regimes of nonlinear interaction that lead to a significant change in electron energy.

5. THE EFFECT OF INTERACTION ON ELECTRON CHARACTERISTICS (THE RESULTS OF SIMULATION BY THE TEST PARTICLE METHOD)

5.1. Interaction regimes

Analysis of the performed simulation shows that the range of resonant energies (about 3–330 keV for $\Theta_X = 44^\circ$) can be divided into four intervals corresponding to qualitatively different characteristics of the interaction. The approximate boundaries of these intervals can be estimated from the dependences of the position of the resonance points $h_R^{(1)}$ and $h_R^{(2)}$ on the energy W_0 (for the considered parameters, the green curve in Fig. 1*b*). The first interval corresponds to low energies in the region where $h_R^{(2)}$ increases with increasing energy ($h_R^{(1)} \approx h_X$), the second interval, to the region where $h_R^{(2)} \approx$ const ($h_R^{(1)} \approx h_X$), and the third interval, to the section in which $h_R^{(2)}$ starts to decrease with increasing energy and $h_R^{(1)}$ increases, but remains close enough to h_X (h_X determines the position of the cutoff point). The last interval corresponds to a small neighborhood of the right-hand boundary of the resonance energy range where the resonance points are fairly close to each other and away from the cutoff point.

As the energy increases, the range of t_0 values corresponding to the efficient resonant interaction (the one that results in a notable change in particle energy) shifts towards the region of greater t_0.

5.1.1. Low energies

Low energies (in a range of approximately 3–70 keV for $\Theta_X = 44^\circ$) correspond to the case where the resonance points are relatively close to each other, the first point being near the cutoff point. In this case (see Fig. 2), there are two regimes of efficient resonant interaction.

For short t_0 ($t_0 \leq 0.02$ s at $W_0 = 50$ keV), the first resonance point is closer to the trailing edge of the wave packet and the second one is outside it (see the red curve in Fig. 2*c*). As a result of the interaction, the untrapped particles lose little energy (bunching in the first resonance region, the red color in Figs. 2*a*

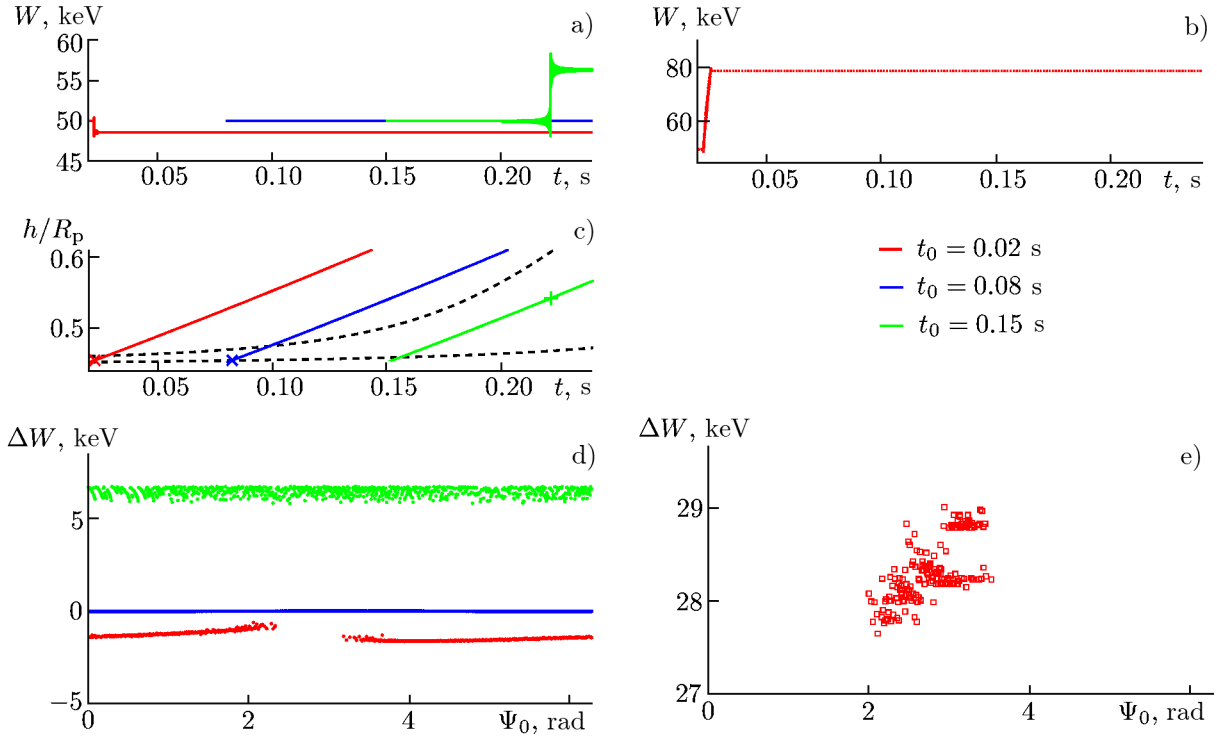

Fig. 2. Interaction regimes as functions of the particle start time t_0 for $W_0 = 50$ keV and $\Theta_X = 44°$. Examples of time dependences of the energy for untrapped (a) and trapped (b) particles, the corresponding trajectories of particles (c) (the markers show the resonance points), and energy variations for untrapped (d) and trapped (e) particles as functions of the initial phase.

and 2d), while the untrapped particles (red color in Figs. 2b and 2d) are accelerated in the first zone and exit from trapping before entering the second zone.

For intermediate values of t_0 ($0.02 < t_0 < 0.15$ s at $W_0 = 50$ keV), both points are located either outside the packet or close to the corresponding edges (the first, to the trailing edge and the second, to the leading edge), i. e., there is a linear interaction with a very small standard deviation (blue color in Figs. 2a, 2c, and 2d).

For long t_0 ($t_0 \approx 0.15$ s at $W_0 = 50$ keV), the first resonance point is located either outside the packet or close to its trailing edge, and the second point is located in the vicinity of the middle of the packet (see the green curve in Figs. 2a and 2d). There are no trapped particles in this case, and the energy of untrapped particles increases (green color in Figs. 2a and 2d). With the increase in $t_0 > 0.15$ s, the second resonance point approaches the trailing edge of the wave packet, which leads first to a smaller acceleration due to bunching and then to a linear interaction with a small standard deviation.

5.1.2. Intermediate energies

Intermediate energies (in a range of approximately 70–200 keV for $\Theta_X = 44°$) correspond to the maximum distance between the resonance points and the maximum (at a constant amplitude) values of the parameters $R^{(1)}$ and $R^{(2)}$. In this case (see Fig. 3), there exists three regimes of efficient resonant interaction.

For short t_0, the first resonance point is closer to the leading edge of the packet and the second one is outside it. Since in this case the amplitude at the resonance point is not maximum and decreases as the particle moves, there are no trapped particles. The energy of the untrapped particles decreases (red color in Figs. 3a, 3c, and 3d). As t_0 increases, regimes similar to those for low energies described in the previous subsection take place.

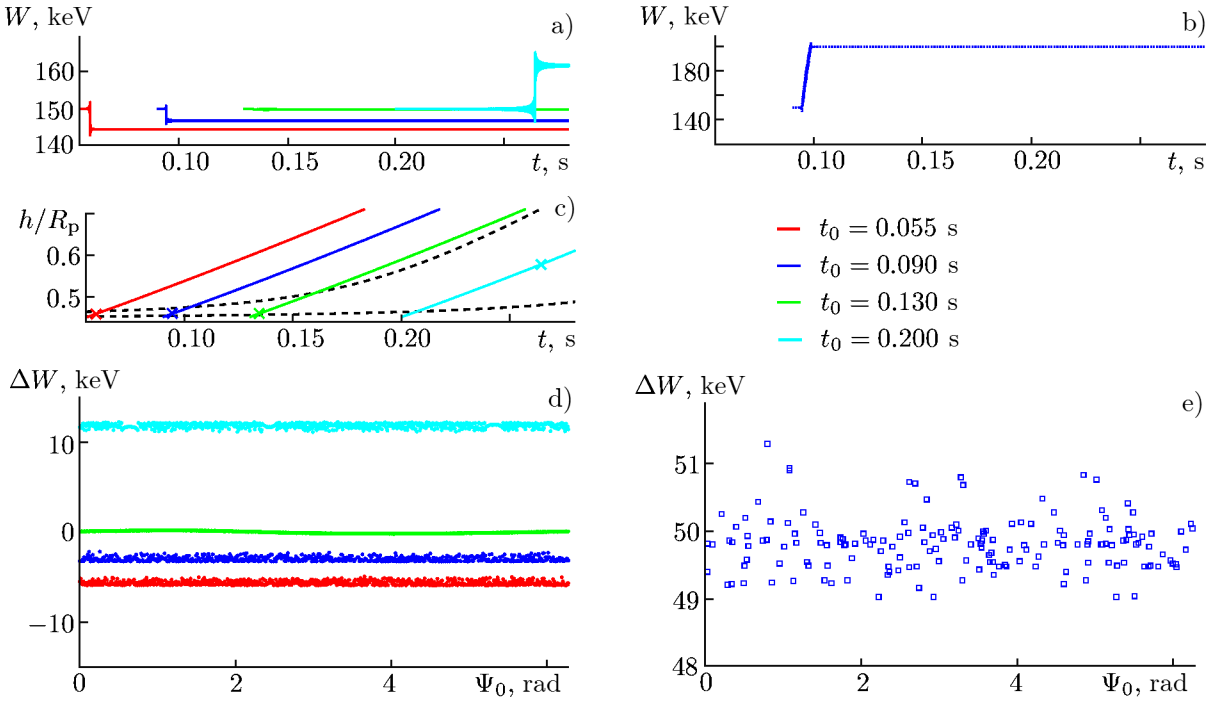

Fig. 3. Interaction regimes as functions of the particle start time t_0 for $W_0 = 150$ keV and $\Theta_X = 44°$. Examples of time dependences of the energy for untrapped (a) and trapped (b) particles, the corresponding trajectories of particles (c) (the markers show the resonance points), and energy variations for untrapped (d) and trapped (e) particles as functions of the initial phase.

5.1.3. High energies

High energies (in a range of about 250 keV for $\Theta_X = 44°$) correspond to a short distance between resonance points, while the point of the first resonance is farther from the cutoff point than in the case of low energies (Fig. 4). In this case, for intermediate values of t_0, there are no cases where both resonance points are outside the packet or near its edges. For any $t_{min} < t_0 < t_{max}$ (t_{min} and t_{max} are, respectively, the minimum and maximum values of t_0 for which efficient resonant interaction is possible), at least one of the resonance points is located in the packet and far enough from its edges.

At $t_0 \approx 0.16$ s, the second resonance point is located close to the leading edge (green curve in Fig. 4c). For untrapped particles, interaction in the second resonance zone is linear with a small standard deviation (green color in Figs. 4a and 4d); the trapped particles exit from trapping after the second resonance zone, but the effect of the latter is small, i. e., the trapping results in acceleration. Quantitatively, this regime differs only slightly from the regime where the second resonance point is outside the packet (blue color); the decrease in the energy of untrapped particles in this case will be smaller, while the acceleration of trapped particles will be greater.

For $t_0 \approx 0.17$ s, both resonance points are far enough from the wave packet edges (blue color) and the result of the interaction is close to the case of a long rectangular packet. Untrapped particles have a bunching in both resonance zones, but acceleration in the second zone is more efficient; the particles are trapped in the first zone and exit from trapping in the second one, but the effect of the second zone prevails, i. e., the particle energy decreases.

As t_0 further increases, interaction in the first resonance zone becomes linear, the trapping of particles is absent, and bunching of untrapped particles, which leads to their acceleration (purple), occurs in the second zone. For $t_0 > 0.22$ s the first resonance point is outside the wave packet and the second one is closer to its trailing edge (yellow curve in Fig. 4c). In this case, the acceleration of untrapped particles due to bunching in the second resonance zone is less effective (yellow color in Figs. 4a and 4d).

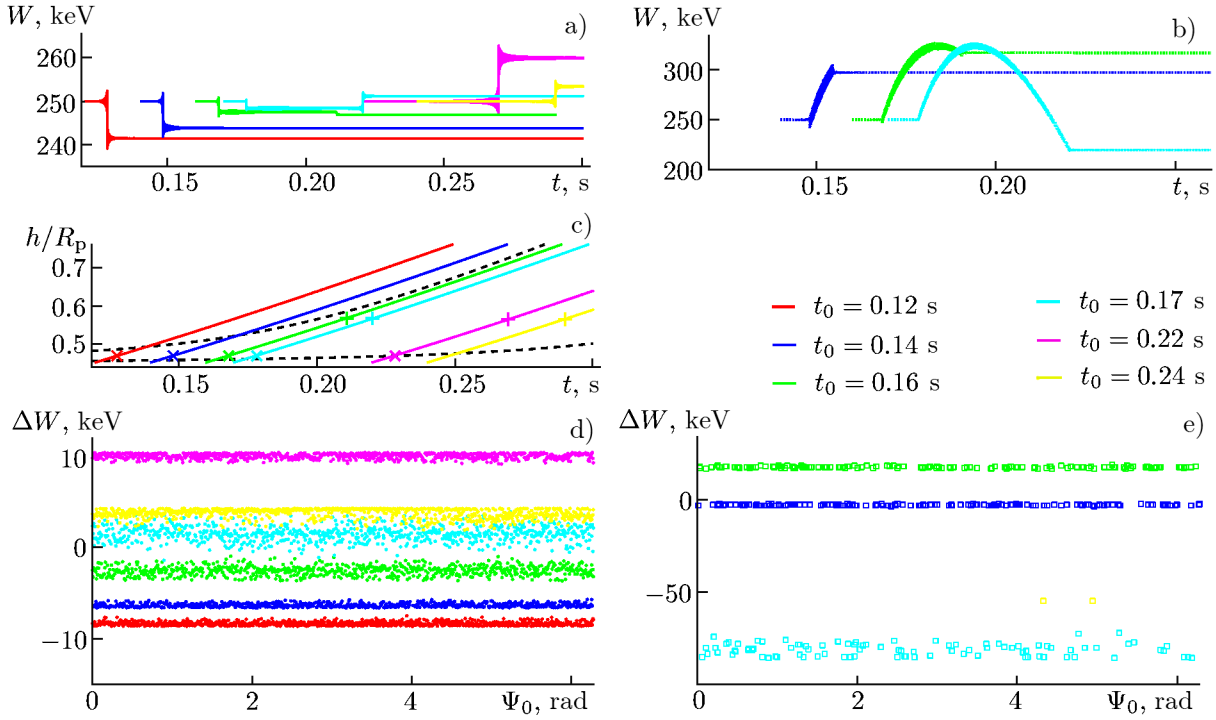

Fig. 4. Interaction regimes as functions of the particle start time t_0 for $W_0 = 250$ keV and $\Theta_X = 44°$. Examples of time dependences of the energy for untrapped (a) and trapped (b) particles, the corresponding trajectories of untrapped particles (c) (the markers show the resonance points), and the energy variations for untrapped (d) and trapped (e) particles as functions of the initial phase.

5.1.4. High energies near the boundary of the resonance range

The vicinity of the right-hand boundary of the resonance energy range is characterized by a short distance between the resonance points and the greatest distance of the first resonance point from the cutoff point (see Fig. 5). The results for this case are presented in Fig. 5.

In the case where both resonance points are inside the packet, but one of them is located near the corresponding edge, the interaction regimes at $W_0 = 300$ keV qualitatively differ from similar regimes for $W = 250$ keV. At $W_0 = 300$ keV, for a certain fraction of particles, trapping takes place in one of the resonant interaction zone and linear interaction occurs in the other zone (blue and purple colors in Figs. 5b and 5d, close-ups are shown on the inserts in Fig. 5b). For shorter t_0, the particles trapped in the first resonance zone have time to exit from trapping (due to the decrease in amplitude) before they reach the second resonance zone. For longer t_0, after the linear interaction with a small standard deviation at the first resonance point the particles turn out to be trapped in the second zone. Accordingly, the particles are accelerated in the first case and lose energy in the second case.

In the case where the particles become trapped in the first resonance zone and exit from trapping after passing the second one, the effect of the second zone prevails, while the decrease in energy can be much more significant than at lower energies (light blue in Figs. 5b and 5d). Recall that at a constant amplitude the parameters $R^{(1)}$ and $R^{(2)}$ decrease as the boundaries of the resonant energy range are approached.

Due to the short distance between resonance points, two regimes that take place for lower energies are absent. They are the trapping of particles in the case where only the first resonance point is located in the packet and a significant acceleration of untrapped particles in the absence of trapping, when only the second resonance point is located in the packet. Trapping in the first resonance zone is possible only for the t_0 values at which both resonance points are in the wave packet. In the case where only the second resonance point is located in the packet, as it approaches the trailing edge of the latter (with increasing t_0), the result

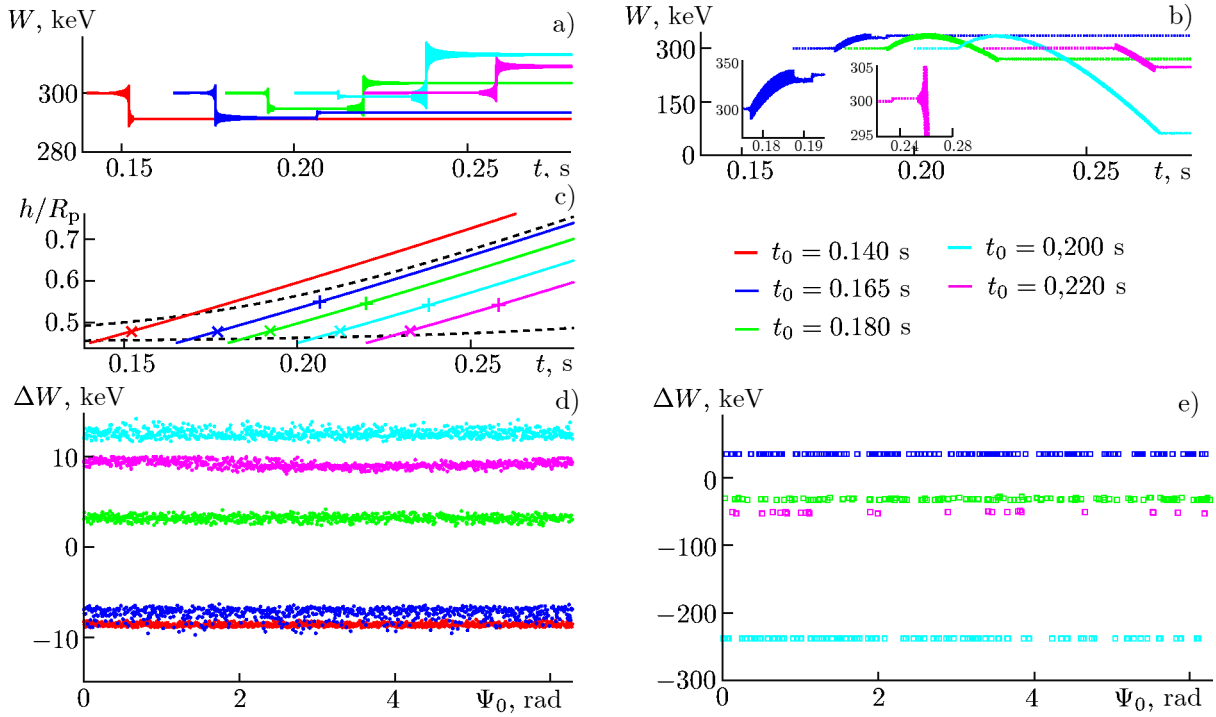

Fig. 5. Interaction regimes as functions of the particle start time t_0 for $W_0 = 300$ keV and $\Theta_X = 44°$. Examples of time dependences of the energy for untrapped (a) and trapped (b) particles, the corresponding trajectories of untrapped particles (c) (the markers show the resonance points), and energy variations for untrapped (d) and trapped (e) particles as functions of the initial phase.

of interaction for untrapped particles is close to linear even in the presence of a small fraction of trapped particles.

Comparison of results for different t_0 and constant energy W_0 permit one to conclude that in the case of a long wave packet covering entirely both zones of resonant interaction, the effects of the resonance zones with opposite signs of effective inhomogeneity counterbalance each other, which leads to a very small final energy variation, both for a single particle and for their ensemble.[1] This is due to the fact that for the considered values of the amplitudes, except for the vicinities of the packet edges, the interaction is strongly nonlinear in both zones.

5.2. Integral characteristics of the interaction

Phase-averaged energy variation $\langle \Delta W \rangle$ and the standard energy deviation σ_W (for the entire ensemble of particles with fixed W_0 and t_0 and separately for untrapped and trapped particles) as functions of the initial energy W_0 and the start time t_0 are presented in Fig. 6. The energy variation averaged over phases and time t_0 and the standard deviation are shown in Fig. 7.

For untrapped particles (Fig. 6a) at short t_0 the value of $\langle \Delta W \rangle^{\rm unt}$ is negative and has a minimum, then, as t_0 increases, it increases and passes to the range of positive values, reaches a maximum and then decreases. Herein, for energies $W_0 < 100$ keV, there is a sufficiently large interval of intermediate values of t_0, where $\langle \Delta W \rangle^{\rm unt} \approx 0$ and $\sigma_W^{\rm unt} < 0.2$ keV. For a fixed energy W_0, the increase in the untrapped-particle energy for longer t_0 slightly exceeds the decrease in energy for shorter t_0. Also, $|\langle \Delta W \rangle^{\rm unt}|$ generally increases with increasing energy.

The interval of t_0 values, in which particles can be trapped by the wave field, exceeds 0.02 s only for high energies $W_0 \geq 200$ keV. For these energy values, $\langle \Delta W \rangle^{\rm tr} > 0$ for shorter t_0 and $\langle \Delta W \rangle^{\rm tr} < 0$ for longer

[1] This conclusion was confirmed by test calculations, the results of which are not shown in this paper for brevity's sake.

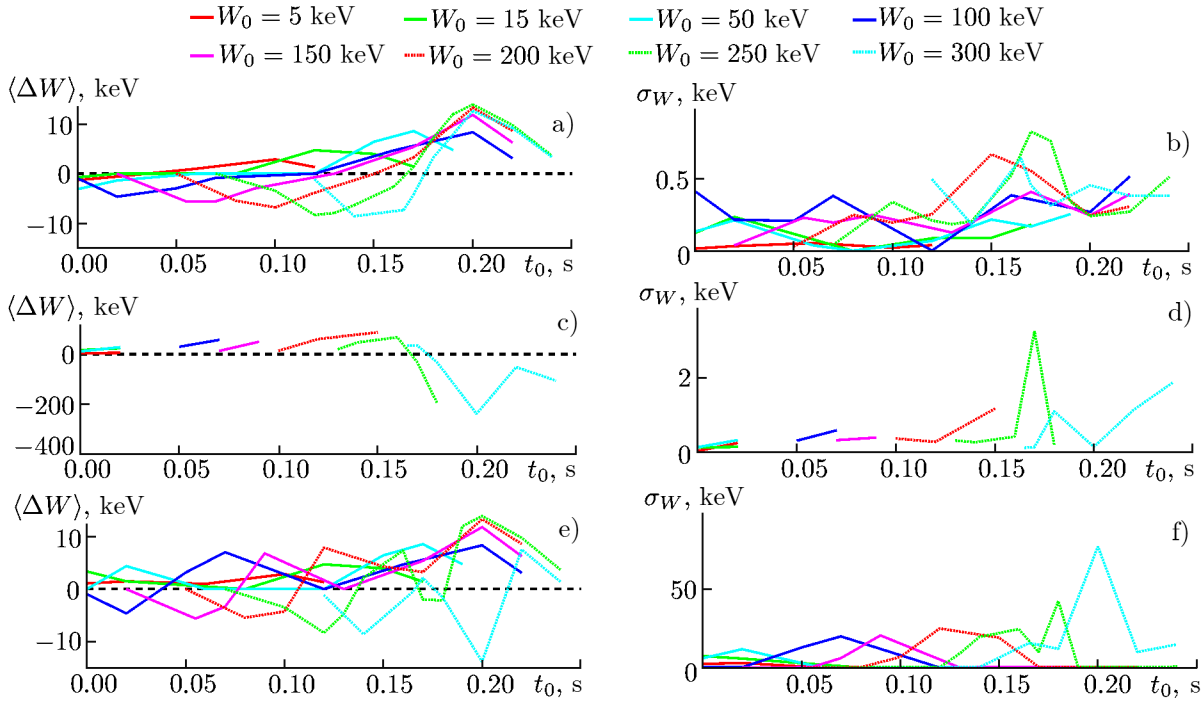

Fig. 6. Mean (a, c, and e) and r. m. s. (b, d and f) energy variations for untrapped particles (a and b), trapped particles (c and d), and the entire ensemble (d and f). $\Theta_X = 44°$.

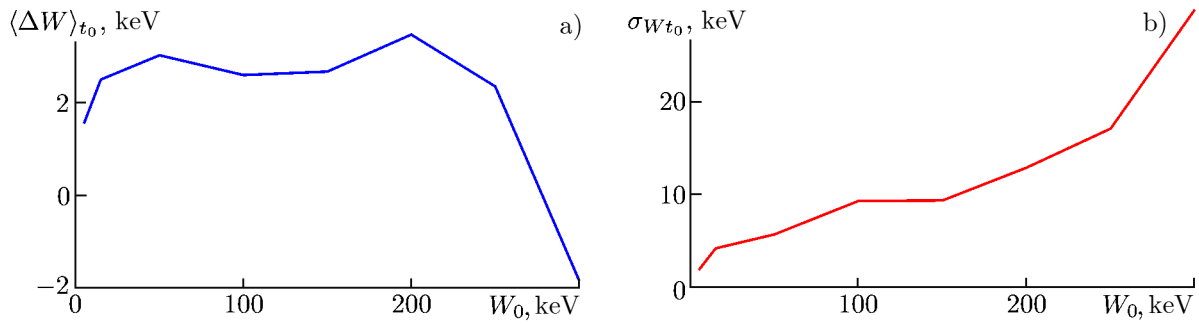

Fig. 7. Energy variation averaged over phases and time t_0 (a) and the corresponding standard deviation (b) as functions of the initial energy. $\Theta_X = 44°$.

t_0. Particles with initial energies $W_0 \leq 200$ keV can only be accelerated as a result of the trapping.

In the presence of trapping, in most cases, the sign of the mean energy variation $\langle \Delta W \rangle$ for the entire ensemble of particles is determined by trapped particles, but since their fraction is small, the absolute value $|\langle \Delta W \rangle|$ is also small, namely, $|\langle \Delta W \rangle| \leq 15$ keV.

For the initial energies $W_0 \leq 250$ keV, the energy variation averaged over phases and start time t_0 ($\langle \Delta W \rangle_{t_0}$) fluctuates in the range 1.5–3.5 keV and the corresponding standard deviation σ_{Wt_0} smoothly increases from 0 to 20 keV. For $W_0 = 300$ keV, we have $\langle \Delta W \rangle_{t_0} \approx -2.0$ keV and $\sigma_{Wt_0} \approx 30$ keV.

On the whole, the performed simulation of the interaction of energetic electrons with a wave packet of radio emission (X mode) of finite duration in the magnetosphere of Tau Bootis b shows the following. In a wide range of initial particle energies W_0 for untrapped particles, the energy of a particle either increases or decreases slightly (up to 5%), depending on its initial position with respect to the wave packet edge. The decrease takes place if the particle is in the packet in the vicinity of the first resonance zone and overtakes the packet before the beginning of the second resonance zone and the increase occurs if the particle catches up with the packet after the latter has left the first resonant-interaction zone and is located in the packet in the vicinity of the second resonant zone. For trapped particles in a wide range of W_0, the energy increases

significantly (from 10 to 100%) if these particles are in the packet in the vicinity of the first resonance zones and overtake the packet before the beginning of the second resonance zone. For high values of W_0, a significant decrease in the energy of particles is also possible as a result of their trapping by the wave field with the predominant effect of the second resonance zone.

For an ensemble of fixed-energy particles distributed in space in the region of resonant interaction, for most of the range of resonant energies, the acceleration of particles will be more efficient than the decrease in their energy. The ensemble of particles with energies in the vicinity of the right-hand boundary of the resonant-energy range, for which the energy decrease will be more efficient, is the exception.

For the considered value of the electron pitch angle at the cutoff point $\Theta_X = 44^\circ$ their significant acceleration is possible in the initial-energy range 10–300 keV. From Fig. 1*b* it follows that this range will decrease, shifting towards the smaller W_0 as Θ_X increases, and will increase (expanding towards the larger W_0) as Θ_X decreases. For the angle $\Theta_X = 33^\circ$ corresponding to the opening angle of the loss cone, significant acceleration is possible for particles with initial energies of up to about 500 keV.

6. DISCUSSION AND CONCLUSIONS

The revealed important properties of the resonant interactions of charged particles (electrons) with radio emission in the magnetospheres of exoplanets are due primarily to a significant difference of the parameters of the magnetic field, plasma, and radio emission from the corresponding parameters in the magnetospheres of the Earth and the planets of the solar system. In particular, the planet Tau Bootis b has a much stronger magnetic field compared with the Earth's magnetosphere, resulting in a higher radio frequency. In this case, the plasma density in the region of radio emission generation is also quite high, i. e., the ratio Ω_p/Ω_c is close in value to a similar parameter in the Earth's magnetosphere. The amplitude of radio emission in the magnetosphere of Tau Bootis b can significantly (by an order of magnitude or more) exceed the AKR amplitude in the Earth's magnetosphere if, in accordance with [10], this radio emission is assumed to be detectable on the Earth with available tools.

These differences lead to the following features of the resonant interaction. First, the distance between resonance points (both in absolute units and in units of wavelength) in the magnetosphere of Tau Bootis b is much greater than in the Earth's magnetosphere. This implies that the wave packets of a realistic duration in the magnetosphere of Tau Bootis b, in contrast to the Earth's magnetosphere [37], cover only one zone of resonant interaction for most of the resonant energies. Secondly, the interaction in both resonance zones will be essentially nonlinear due to the high amplitude for most of the resonant energies (recall that in the Earth's magnetosphere a strong nonlinearity is possible only in the second resonance zone).

Strong nonlinearity, in turn, leads to a more important role of the effects of trapping of particles by the wave field. When interacting with short packets, the trapping effects can lead to a drastic (from 10 to 100%) acceleration of particles in a wide energy range from tens to hundreds of kiloelectronvolts.

This is exactly a case that takes place for the plasma and magnetic-field parameters corresponding to modern ideas about the magnetosphere of the exoplanet Tau Bootis b. Thus, in this paper, we have demonstrated the possibility of nonlinear acceleration of energetic (with energies of the order 10–500 keV) electrons in the magnetosphere of this exoplanet by the field of its radio emission with the energy gain reaching up to 100% with respect to the initial energy.

Note that the considered interaction occurs, partially or completely, in the region of radio emission generation. If it is assumed that radio emission in the magnetosphere of Tau Bootis b is generated as a result of cyclotron instability, then in the process of generation part of the ensemble of energetic electrons gives energy to the wave and the shape of the wave packet changes. For a correct assessment of the total energy balance in the system, it is necessary to analyze the evolution of the electron distribution function, and in prospect it is needed to consider a self-consistent problem with allowance for the evolution of the wave packet in the generation region.

This work was supported by the Ministry of Education and Science of the Russian Federation (agreement No. 075–15–2020–780).

REFERENCES

1. V. G. Surdin, *Radiophys. Quantum Electron.*, **63**, Nos. 9–10, 656–672 (2021). https://doi.org/10.1007/s11141-021-10088-6
2. https://exoplanets.nasa.gov/discovery/exoplanet-catalog/
3. J.-M. Grießmeier, S. Preusse, M. Khodachenko, et al., *Planet. Space Sci.*, **55**, No. 5, 618–630 (2007). https://doi.org/10.1016/j.pss.2006.01.008
4. J.-M. Grießmeier, P. Zarka, and H. Spreeuw, *Astron. Astrophys.*, **475**, No. 1, 359–368 (2007). https://doi.org/10.1051/0004-6361:20077397
5. J.-M. Grießmeier, P. Zarka, and J. M. Girard, *Radio Sci.*, **46**, No. 5, RS0F09 (2011). https://doi.org/10.1029/2011RS004752
6. A. Reiners and U. R. Christensen, *Astron. Astrophys.*, **522**, A13 (2010). https://doi.org/10.1051/0004-6361/201014251
7. K. G. Kislyakova, M. Holmström, H. Lammer, et al., *Science*, **346**, No. 6212, 981–984 (2014). https://doi.org/10.1126/science.1257829
8. C. Weber, H. Lammer, I. F. Shaikhislamov, et al., *Mon. Notices Royal Astron. Soc.*, **469**, No. 3, 3505–3517 (2017). https://doi.org/10.1093/mnras/stx1099
9. C. Weber, N. V. Erkaev, V. A. Ivanov, et al., *Mon. Notices Royal Astron. Soc.*, **480**, No. 3, 3680–3688 (2018). https://doi.org/10.1093/mnras/sty2079
10. J. D. Turner, P. Zarka, J.-M. Grießmeier, et al., *Astron. Astrophys.*, **645**, A59 (2021). https://doi.org/10.1051/0004-6361/201937201
11. E. A. Benediktov, G. G. Getmantsev, Yu. A. Sazonov, and A. F. Tarasov, *Kosm. Issled.*, **3**, No. 4, 614–617 (1965).
12. D. A. Gurnet, *J. Geomagn. Geoelectr.*, **30**, No. 3, 257–272 (1978). https://doi.org/10.5636/jgg.30.257
13. C. S. Wu and L. C. Lee, *Astrophys. J.*, **230**, 621–626 (1979). https://doi.org/10.1086/157120
14. P. L. Pritchett, *J. Geophys. Res. Space Phys.*, **89**, No. A10, 8957–8970 (1984). https://doi.org/10.1029/JA089iA10p08957
15. V. Yu. Trakhtengerts and M. J. Rycroft, *Whistler-Mode and Alfvén Cyclotron Masers in Space*, Cambridge University Press, Cambridge (2008).
16. B. F. Burke and K. L. Franklin, *J. Geophys. Res.*, **60**, No. 2, 213–217 (1955). https://doi.org/10.1029/JZ060i002p00213
17. V. V. Zheleznyakov, *Astron. Zhurn.*, **42**, No. 4, 798–809 (1965).
18. P. Zarka, *J. Geophys. Res. Planets*, **103**, No. E9, 20159–20194 (1998). https://doi.org/10.1029/98JE01323
19. D. S. Bisikalo and V. I. Shematovich, *Astron. Rep.*, **59**, No. 9, 836–842 (2015). https://doi.org/10.1134/S1063772915090024
20. P. A. Bespalov and V. Yu. Trakhtengerts, *Alfvén Masers* [in Russian], Inst. Prikl. Fiz. AN SSSR, Gorky (1986).
21. W. Li and M. K. Hudson, *J. Geophys. Res. Space Phys.*, **124**, No. 11, 8319–8351 (2019). https://doi.org/10.1029/2018JA025940

22. V. E. Shaposhnikov and V. V. Zaitsev, *Planet. Space Sci.*, **41**, No. 5, 341–346 (1993). https://doi.org/10.1016/0032-0633(93)90067-C

23. V. Y. Trakhtengerts, *J. Geophys. Res. Space Phys.*, **100**, No. 9, 17205–17210 (1995). https://doi.org/10.1029/95JA00843

24. Y. Hobara, V. Y. Trakhtengerts, A. G. Demekhov, and M. Hayakawa, *J. Geophys. Res. Space Phys.*, **103**, No. 9, 20449–20458 (1998). https://doi.org/10.1029/98JA01746

25. A. G. Demekhov, D. Nunn, and V. Y. Trakhtengerts, *Phys. Plasmas*, **10**, No. 11, 4472–4477 (2003). https://doi.org/10.1063/1.1620507

26. O. Santolík, D. A. Gurnett, J. S. Pickett, et al., *J. Geophys. Res. Space Phys.*, **114**, No. A12, A00F03 (2009). https://doi.org/10.1029/2009JA014586

27. D. Shklyar and H. Matsumoto, *Surveys in Geophysics*, **30**, No. 2, 55–104 (2009). https://doi.org/10.1007/s10712-009-9061-7

28. V. Trakhtengerts and A. Demekhov, *J. Atm. Solar-Terr. Phys.*, **69**, No. 14, 1651–1656 (2007). https://doi.org/10.1016/j.jastp.2007.02.009

29. Y. Omura, J. Pickett, B. Grison, et al., *J. Geophys. Res. Space Phys.*, **115**, A07234 (2010). https://doi.org/10.1029/2010JA015300

30. M. Shoji, Y. Omura, B. Grison, et al., *Geophys. Res. Lett.*, **38**, No. 17, L17102 (2011). https://doi.org/10.1029/2011GL048427

31. J. M. Albert and J. Bortnik, *Geophys. Res. Lett.*, **36**, No. 12, L12110 (2009). https://doi.org/10.1029/2009GL038904

32. Y. Kubota and Y. Omura, *J. Geophys. Res. Space Phys.*, **122**, No. 1, 293–309 (2017). https://doi.org/10.1002/2016JA023267

33. V. S. Grach and A. G. Demekhov, *J. Geophys. Res. Space Phys.*, **125**, No. 2, e2019JA027358 (2020). https://doi.org/10.1029/2019JA027358

34. P. L. Pritchett, R. J. Strangeway, R. E. Ergun, and C. W. Carlson, *J. Geophys. Res. Space Phys.*, **107**, No. A12, 1437 (2002). https://doi.org/10.1029/2002JA009403

35. T. M. Burinskaya and J. L. Rauch, *Plasma Phys. Rep.*, **33**, No. 1, 28–37 (2007). https://doi.org/10.1134/S1063780X07010047

36. T. M. Burinskaya and M. M. Shevelev, *Plasma Phys. Rep.*, **42**, No. 10, 929–935 (2016). https://doi.org/10.1134/S1063780X16100020

37. V. S. Grach and A. G. Demekhov, *Radiophys. Quantum Electron.*, **63**, No. 3, 157–176 (2020). doi10.1007/s11141-021-10043-5173–194

38. V. S. Grach and A. G. Demekhov, *Radiophys. Quantum Electron.*, **63**, No. 11, 827–847 (2021). doi10.1007/s11141-021-10098-4

39. V. I. Karpman, Y. N. Istomin, and D. R. Shklyar, *Plasma Phys.*, **16**, No. 8, 685–703 (1974). https://doi.org/10.1088/0032-1028/16/8/001

40. J. M. Albert, *Phys. Fluids B.*, **5**, No. 8, 2744–2750 (1993). https://doi.org/10.1063/1.860715

41. J. M. Albert, *J. Geophys. Res. Space Phys.*, **105**, No. A9, P.21191–21209 (2000). https://doi.org/10.1029/2000JA000008

42. A. G. Demekhov, V. Yu. Trakhtengerts, M. J. Rycrott, and D. Nunn, *Geomagn. Aeron.*, **46**, No. 6, 711–716 (2006). https://doi.org/10.1134/S0016793206060053

43. V. S. Grach and A. G. Demekhov, *Radiophys. Quantum Electron.*, **60**, No. 12, 942–959 (2018). https://doi.org/10.1007/s11141-018-9860-0

44. D. A. Gurnett, R. R. Anderson, F. L. Scarf, et al., *Space Sci. Rev.*, **23**, No. 1, 103–122 (1979). https://doi.org/10.1007/BF00174114

45. D. A. Gurnett and R. R. Anderson, in: S. Akasofu and J. Kan, eds., *Geophys. Monograph Series, Vol. 25, Physics of Auroral Arc Formation*, American Geophysical Union, Washington (1981), pp. 341–350. https://doi.org/10.1029/GM025p0341

46. A. Morioka, H. Oya, and S. Miyatake, *J. Geomagn. Geoelectr.*, **33**, No. 1, 37–62 (1981). https://doi.org/10.5636/jgg.33.37

47. J. D. Menietti, A. M. Persoon, J. S. Pickett, and D. A. Gurnett, *J. Geophys. Res. Space Phys.*, **105**, No. A8, 18857–18866 (2000). https://doi.org/10.1029/1999JA000389

48. V. Y. Trakhtengerts, A. G. Demekhov, E. E. Titova, et al., *Phys. Plasmas*, **11**, No. 4, 1345–1351 (2004). https://doi.org/10.1063/1.1667495

49. X. J. Zhang, D. Mourenas, A. V. Artemyev, et al., *Geophys. Res. Lett.*, **47**, No. 15, e88853 (2020). https://doi.org/10.1029/2020GL088853

50. D. Nunn, X. J. Zhang, D. Mourenas, A. V. Artemyev, et al., *Geophys. Res. Lett.*, **48**, No. 7, e92178 (2021). https://doi.org/10.1029/2020GL092178

51. R. L. Mutel, W. M. Peterson, T. R. Jaeger, and J. D. Scudder, *J. Geophys. Res. Space Phys.*, **112**, No. A7, A07211 (2007). https://doi.org/10.1029/2007JA012442

52. A. G. Demekhov, V. Yu. Trakhtengerts, M. Rycroft, and D. Nunn, *Geophys. Aeron.*, **49**, No. 1, 24–29 (2009). https://doi.org/10.1134/S0016793209010034

53. Y. Omura and Q. Zhao, *J. Geophys. Res. Space Phys.*, **117**, No. A8, A08227 (2012). https://doi.org/10.1029/2012JA017943

54. D. R. Shklyar, in: eds. L. M. Zelenyi and I. S. Veselovsky, *Plasma Geliogeophysics, Vol. II* [in Russian], Fizmatlit, Moscow (2008), pp. 391–490.

55. J. M. Albert, X. Tao, and J. Bortnik, in: D. Summers, I. R. Mann, D. N. Baker, and M. Schulz, eds., *Geophys. Monograph Series, Vol. 199, Dynamics of the Earth's Radiation Belts and Inner Magnetosphere*, American Geophysical Union, Washington (2012), pp. 255–264. https://doi.org/10.1029/2012gm001324

56. V. S. Grach, A. G. Demekhov, and A. V. Larchenko, *Earth, Planets and Space*, **73**, No. 1, 129 (2021). https://doi.org/10.1186/s40623-021-01453-w